AFRL-RD-PS-
TR-2020-0042

NOVEL DETECTION OF OPTICAL ANGULAR MOMENTUM

David Voelz

Klipsch School of ECE
New Mexico State University
MSC 3-0, PO Box 30001
Las Cruces, NM 88003

12 April 2017

Final Report

AIR FORCE RESEARCH LABORATORY
Directed Energy Directorate
3550 Aberdeen Ave SE
AIR FORCE MATERIEL COMMAND
KIRTLAND AIR FORCE BASE, NM 87117-5776

NOTICE AND SIGNATURE PAGE

AFRL-RD-PS-TR-2020-0042 HAS BEEN REVIEWED AND IS APPROVED FOR PUBLICATION IN ACCORDANCE WITH ASSIGNED DISTRIBUTION STATEMENT.

//Charlie T. Bellows//

CHARLIE T BELLOWS, Lt Col, USAF PhD
Chief Engineer, AFRL/RDS

REPORT DOCUMENTATION PAGE

Form Approved
OMB No. 0704-0188

1. REPORT DATE ***(DD-MM-YYYY)***	**2. REPORT TYPE**	**3. DATES COVERED** ***(From - To)***
12-04-2017	FINAL REPORT	09-30-2014 – 9/30/2016

4. TITLE AND SUBTITLE

Novel Detection of Optical Orbital Angular Momentum

5a. CONTRACT NUMBER
FA9451-14-1-0292

5b. GRANT NUMBER

5c. PROGRAM ELEMENT NUMBER

6. AUTHOR(S)
David Voelz

5d. PROJECT NUMBER

5e. TASK NUMBER

5f. WORK UNIT NUMBER

7. PERFORMING ORGANIZATION NAME(S) AND ADDRESS(ES)
Klipsch School of ECE
New Mexico State University
MSC 3-0, PO Box 30001
Las Cruces, NM 88003

8. PERFORMING ORGANIZATION REPORT NUMBER

9. SPONSORING / MONITORING AGENCY NAME(S) AND ADDRESS(ES)
Air Force Research Laboratory
3550 Aberdeen Ave SE
Kirtland AFB, NM 87117-5776

10. SPONSOR/MONITOR'S ACRONYM(S)
AFRL/RDSS

11. SPONSOR/MONITOR'S REPORT NUMBER(S)
AFRL-RD-PS-TR-2020-0042

12. DISTRIBUTION / AVAILABILITY STATEMENT

Approved for public release; distribution is unlimited. Public Affairs Release Approval: AFRL-2020-0107

13. SUPPLEMENTARY NOTES

14. ABSTRACT

The work reported here includes two investigations related to the study and measurement of orbitalangular momentum (OAM): (I) a characterization of the variation of photonic orbital angular momentum (POAM) under Compton scattering, and (II) a design of new plasmonic metasurfaces that convert optical vortex beams into surface plasmon polaritons (SPPs).

15. SUBJECT TERMS

Orbital Angular Momentum (OAM), Photonic Orbital Angular Momentum (POAM), Compton Scattering, Surface Plasmon Polaritons (SPPs)

16. SECURITY CLASSIFICATION OF:			**17. LIMITATION**	**18. NUMBER OF PAGES**	**19a. NAME OF RESPONSIBLE PERSON** Charlie Bellows
a. REPORT Unclassified	**b. ABSTRACT** Unclassified	**c. THIS PAGE** Unclassified	SAR	19	**19b. TELEPHONE NUMBER** ***(include area code) 505-846-7963***

Standard Form 298 (Rev. 8-98)
Prescribed by ANSI Std. 239.18

TABLE OF CONTENTS

LIST OF FIGURES

1.0 SUMMARY

The work reported here includes two investigations related to the study and measurement of orbital angular momentum (OAM): (I) a characterization of the variation of photonic orbital angular momentum (POAM) under Compton scattering, and (II) a design of new plasmonic metasurfaces that convert optical vortex beams into surface plasmon polaritons (SPPs).

2.0 INTRODUCTION

Photons can carry both spin and orbital angular momentum (OAM).[1] Spin angular momentum is associated with the polarization of the optical field whereas OAM involves a singularity associated with a dark spot in the intensity distribution and an azimuthal dependence of the wave phase front. The azimuthal dependence is typically a helical wavefront and is mathematically given by a complex exponential term with multiple OAM states or topological charges.[2, 3] This singularity structure is often called an optical vortex. The polarization of a photon provides a two dimensional Hilbert space. But in principle, OAM is associated with the spatial distribution of the wave function and has an infinite number of eigenstates.[4-8] Thus, OAM can be exploited in optical communication applications to increase the information carrying capacity of a beam. Optical beams that involve OAM include Laguerre-Gaussian beam modes, Bessel beams, Hermite-Bessel beams, Airy beams and helical Mathieu beams.

Encoding information for optical communications is a direct application of OAM. In this case, the OAM of an optical beam or wave is artificially manipulated. However, OAM characteristics also arise naturally in other situations such as the propagation of an optical field through atmospheric turbulence.[9] Interaction with the refractive index variations of turbulent air can result in the creation of branch points pairs (two coupled, counter rotating helical phase structures) in the propagated field. These branch points are indicative of optical OAM. Recently, the type of field that leads to the formation of a pair of branch points has been identified.[10] Furthermore, the abundance and spacing of branch point pairs in the received optical field can be related to the turbulence strength and extent.[11] This relationship can be studied to gain a better understanding of turbulence and improved mitigation techniques, or it could even be applied as a diagnostic measurement approach.

Although the singularity points (zero intensity) associated with OAM are not directly measurable due to the finite size of a measurement pixel, the helical phase around the point can be observed with interferometric or wavefront sensing approaches. Measurement methods that have been proposed include: (a) conversion of the helical wavefront to a planar wavefront using a holographic element and then focusing the result through a pinhole or to a fiber optic,[12] (b) circular dichroism angle resolved photoemission;[13] (c) interfering the input wave with an inverted or rotated copy of itself. This approach has been developed into a concept of cascaded of Mach-Zehnder interferometers for measuring the OAM of single photons;[14] (d) where in simulation a more complex computer-generated hologram has been demonstrated that can detect several different states but with an efficiency that cannot exceed the reciprocal of the number of states.[15] A typical example of an interferometric approach related to methods (a) and (c) and (d) is the concept of interfering a beam, described by a complex phase front $\exp(im\varphi)$, with its mirror image. This produces an interferogram with $2m$ radial spokes. A computer-generated hologram with a fork-dislocation introduces a helical phase front in the diffracted beam. This type of hologram can be used to create a beam with OAM or, when operated in reverse, the hologram can flatten an input helical phase front. These techniques allow photons to be tested only for particular OAM states but they involve tabletop-sized interferometric setups and elements such as holograms, dove prisms and beam splitters. The efficiency of the holographic approaches also tends to be low.

3.0 METHODS, ASSUMPTIONS, AND PROCEDURES

Previous work related to this effort included a new characterization of the influence of atmospheric turbulence on light OAM, a study of interferometic OAM measurement error, and the investigation of transferring OAM from photons to electrons. The objective of the work reported here is two-fold: 1) to consider the interaction of photons and electrons under Compton scattering to help understand this mechanism in terms of OAM detection, and 2) develop a photonic device concept for potential OAM detection.

3.1 *Characterize of OAM under Compton scattering*.

In this part of the study, we briefly analyze a change in the OAM of twisted light in a Compton scattering situation by evaluating the associated scattering matrix within a semi classical physics framework. This work illustrates the possibility for OAM to be transferred through scattering to atomic electrons. It also emphasizes the conservation of total angular momentum in the exchange of OAM to the relatively massive electrons. An analytical expression is evaluated for the scattering matrix of Compton scatter for twisted light. The expression is valid for any axial symmetric beam that carries well defined OAM. In addition, two different beam types are examined and related numerical calculations are implemented.

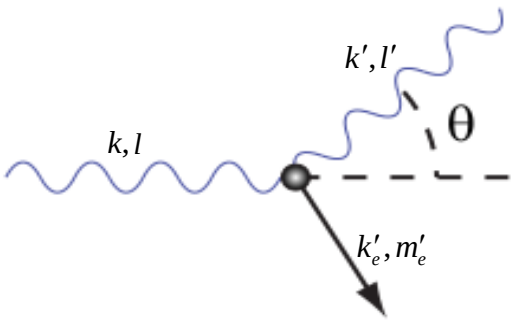

Figure 1. Schematic of Compton scattering with associated parameters.

The schematic diagram of Compton scattering in Fig. 1 identifies the scattered photonic wave number (k) as well as the OAM topical charge (l) by primed parameters, while the associated wave number and orbital angular momentum of the recoil electron is indicated by k_e' and m_e', respectively. The scattering angle (θ) is defined as the angle between the incident beam and the scattering direction. The analysis is based on a semi classical evaluation of the scattering matrix of Compton scatter and illustrates the fundamental exchange the orbital angular momentum between the twisted light wave and the electrons.

The Compton scattering matrix is defined as $S = \left\langle f' \middle| e^{i(\vec{k}'-\vec{k}).\vec{r}} \middle| f \right\rangle$ where f' and f represent the scattered and initial state of the system, $\vec{k}$, $\vec{k}'$ are the incident and scattered wave vectors, and $\vec{r}$ is a position vector.[16] The cylindrical coordinates are applied such that the optical axis is along the z-axis. In this analysis, both the spatial electronic and photonic wave functions, Φ and Ψ, are considered so the Compton scattering matrix can be described as

$$S = \left\langle \Phi^*(\vec{r}')\Psi^*(\vec{r}') \middle| e^{i(\vec{k}'-\vec{k}).\vec{r}} \middle| \Phi(\vec{r})\Psi(\vec{r}) \right\rangle, \tag{1}$$

where * indicates the conjugate, and

$$\Phi(\vec{r}) = P_m(\rho, z)e^{-im\varphi}, \text{ and} \tag{2}$$

$$\Psi(\vec{r}) = R_l(\rho, z)e^{-il\varphi}, \tag{3}$$

where m and l indicate the electronic state and the OAM state, respectively. Due to the azimuthal symmetry of twisted light, normalized wave functions in cylindrical coordinates are applied in Eq. (1). Substituting Eqs. (2) and (3) into Eq. (1) yields

$$S = \left\langle P^*_{m'}(\rho', z')e^{i(m'+l')\varphi}R^*_{l'}(\rho', z') \middle| e^{i(\vec{k}'-\vec{k}).\vec{r}} \middle| P_m(\rho, z)e^{-i(m+l)\varphi}R_l(\rho, z) \right\rangle, \tag{4}$$

Reorganizing Eq. (4) leads to

$$S = \left\langle P^*_{m'}(\rho', z')R^*_{l'}(\rho', z') \middle| e^{i(\vec{k}'-\vec{k}).\vec{r}} \middle| P_m(\rho, z)R_l(\rho, z) \right\rangle \left\langle e^{i(\Delta m+\Delta l)\varphi} \right\rangle. \tag{5}$$

where $\Delta m = m' - m$ and $\Delta l = l' - l$; these represent the change in the electronic and the OAM state due to the scattering process. The last angle bracket of Eq. (5) is evaluated directly using the Dirac delta function,

$$\left\langle e^{i(\Delta m+\Delta l)\varphi} \right\rangle = \delta(\Delta m + \Delta l). \tag{6}$$

Eq. (6) shows that a decrease in OAM is equivalent to an increase of its electron counterpart, $\Delta m = -\Delta l$. Consequently, the Compton scattering matrix is not terminated as long as OAM exchanges between the photon and the electron and is conserved through scattering.

Evaluating the Compton scattering matrix requires resolving the wave functions as well as the middle exponential term. The electronic radial wave function $P_m(\rho, z)$ is a separable and generally given by

$$P_m(\rho, z) = J_m(\kappa_e\rho)e^{ik_e z}, \tag{7}$$

where J_m is the Bessel function, κ_e and k_e are transverse and longitudinal electronic pointing vectors, respectively. On the other hand, the wave vector of collimated twisted light is generally composed of two components – orbital and longitudinal [17] and can be presented as

$$\vec{k} = \kappa\hat{\varphi} + k\hat{z}. \tag{8}$$

Hence, the middle term in the scattering matrix in Eq. (5) is simplified as

$$\exp[i(\vec{k}' - \vec{k}).\vec{r}] = \exp[i(k' - k)z]. \tag{9}$$

Equations (6), (7) and (9) are implemented to define the scattering matrix as follow

$$S = \left\langle J^*_{m'}(\kappa'_e\rho')R^*_l(\rho', z') \middle| J_m(\kappa_e\rho)R_l(\rho, z) \right\rangle \delta(\Delta k_e + \Delta k). \tag{10}$$

The Dirac delta term indicates that the longitudinal component of the pointing vector, which represents the linear momentum, is also exchanged between the electron and the photon. An increase of the linear momentum of the electron is equivalent to decreasing the photon linear momentumn, which is consistent with the well-known Compton's formula.[18] Conservation of both linear and orbital momentum emphasizes the conservation of the total momentum for twisted photons in Compton scattering.

Our objective is to focus on the change of photonic orbital angular momentum in Compton scattering. The analysis leads to evaluating the scattering matrix regardless of the initial OAM state. It is computed for a given change in OAM relative to the zero order state or "untwisted mode" i.e.:

$$S = \left\langle J^*_{\Delta l}(\kappa'\rho) R^*_{\Delta l}(\rho, z') \middle| J_0(\kappa\rho) R_0(\rho, z) \right\rangle. \tag{11}$$

The assumptions for Eqs. (5) and (9) are that there is no change in radial parameter (ρ) through scattering and the axial parameter (z) depends only on the scattering angle (θ). As a result, the scattering matrix is evaluated for a specific axial distance.

3.2 Design of a plasmonic metasurface to measure OAM.

Optical vortex beams have opened up novel applications in optical communications, optical trapping and imaging, and even quantum information processing. Efficient detection of OAM in light beams is imperative for these applications; however, it is challenging task.[19] Recently, metasurfaces have received considerable attention as elements for optical sensing systems due to their properties of increased operational bandwidth and reduced loss.[20, 21] Plasmonic metasurfaces are broadly defined as two-dimensional metamaterials constructed with a periodic or a random arrangement of subwavelength building blocks, or meta-atoms.[22, 23] The optical properties of metasurfaces can be precisely tailored through the engineered interaction of meta-atoms with light, allowing control of the spatial distribution of the fundamental electromagnetic properties: permittivity ε and permeability μ.

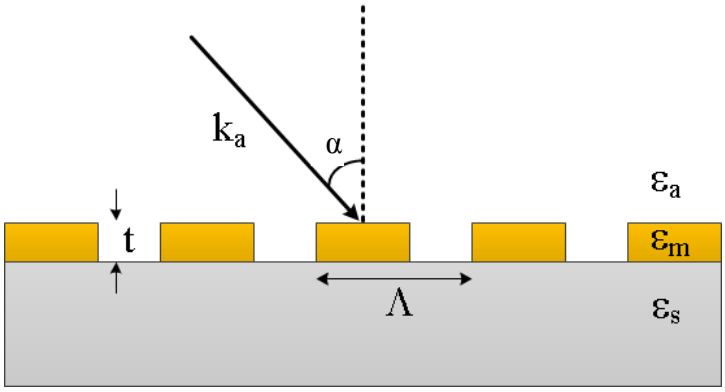

Figure 2. Metasurface illustration: k_a – incident light; α – incident angle; t – metal layer thickness; Λ – period of metasurface; ε_a, ε_m, ε_s – emissivity of air, metal, and the substrate, respectively.

In this study, we report a new plasmonic metasurface design that can potentially convert optical vortex beams into surface plasmon polaritons (SPPs). A typical metasurface is illustrated in Fig. 2 and is composed of free space or air (ε_a), a periodic subwavelength metal (ε_m) layer and the substrate (ε_s). The structure resonantly couples to the electric and/or magnetic components of the incident light k_a and exhibits properties that are not found in nature. It excites surface waves, which are known as surface

plasmon polaritons (SPPs) and they are scattered by variation in the surface impedance to produce a desired radiation output. The excitation satisfies the phase-matching condition

$$k_{spp} = k_a \sin\alpha \pm \Delta k, \tag{12}$$

where k_{SPP} is the electromagnetic field of the surface waves and the net momentum Δk provided by the metasurface is related to the phase gradient. The dispersion relationship of the surface plasmon wave in the thin metal films satisfies

$$\exp(2tk_m) = \frac{(k_m\varepsilon_a - k_a\varepsilon_m)(k_m\varepsilon_s - k_s\varepsilon_m)}{(k_m\varepsilon_a + k_a\varepsilon_m)(k_m\varepsilon_s + k_s\varepsilon_m)}, \tag{13}$$

where

$$k_i^2 = k_{spp}^2 - k_0^2\varepsilon_i,\ i = a, m, s. \tag{14}$$

In addition, the dielectric constant of a real metal is [24]

$$\varepsilon_m = \varepsilon_{intraband,f} + \varepsilon_{interband,f} = 1 - \frac{\omega_p^2}{\omega(\omega - j\Gamma\omega)} + \sum_{m=1}^{k} \frac{\omega_p'^2}{(\omega_m^2 - \omega^2) + j\Gamma_m\omega}, \tag{15}$$

This expression includes both intraband and interband transitions, which are the two most important processes involved in the study of its electronic properties.

The proposed metasurface design structure is demonstrated in Fig. 3(a). An incident optical vortex is coupled into resonant surface plasmon waves via a circular resonator. When an optical vortex beam $k_a(r, \varphi)$ in free space is not able to provide enough momentum to directly launch SPPs on a metal surface, the extra momentum K_G that is introduced by the proposed structure can overcome this challenge. Referring to Eq. (12) and assuming a normally incidence vortex beam, the phase-matching condition is modified as

$$\vec{\mathbf{k}}_a(r,\varphi) + \vec{\mathbf{K}}_G(r,\varphi) = \vec{\mathbf{k}}_{SPP}, \tag{16}$$

where K_G in the proposed structure is

$$\vec{\mathbf{K}}_G(r,\varphi) = \frac{2\pi}{r\varphi}N, \tag{17}$$

and N is an integer. Specifically, as a vortex beam is normally incident on the metasurface, is excites two counter propagating surface waves from two small portions of the angular field components of the incident vortex beam, η_1 and η_2, as illustrated in Fig. 3(b). The resulting surface wave η_t is a superposition of the two components with $\eta_t = \eta_1 + \eta_2$. Hence, the total field intensity at the center of the metasurface, I_t, is determined by the relative phase difference between the two components, that is,

$$I_t \propto \eta_t\eta_t^* \tag{18}$$

where * indicates the complex conjugate.

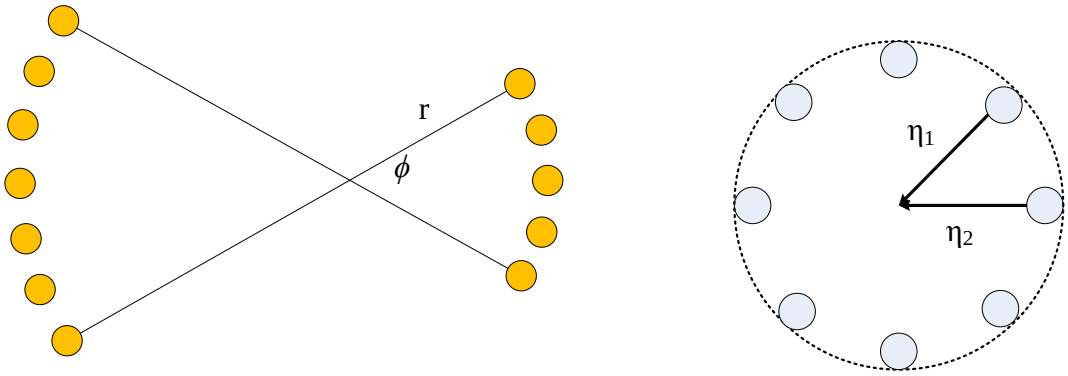

(a) (b)

Figure 3. (a) Proposed metasurface structure. Note: r – radius; ϕ – angle; (b) two example counter surface waves η_1 and η_2 that are excited from a vortex beam.

4.0 RESULTS AND DISCUSSION

The following subsections describe the primary results achieved for the two topics introduced in Section 3. More details can be found in the articles [25, 26].

4.1 Characterization of OAM under Compton scattering

The scattering matrix of Eq. (11) is calculated for two twisted light beams: a Laguerre Gaussian (LG) beam and a Bessel Gaussian (BG) beam. The spatial wave function of the LG beam is given by [27]

$$R_l^{LG}(\rho,z)=\frac{C_p^l}{w(z)}\left[\frac{\sqrt{2}\rho}{w(z)}\right]^{|l|}\exp\left(-\frac{\rho^2}{w(z)^2}\right)L_p^{|l|}\left(\frac{2\rho^2}{w(z)^2}\right)\exp\left[\frac{ik\rho^2 z}{2(z^2+z_R^2)}+iG_q^{|l|}(z)\right], \tag{19}$$

where $C_p^{\,i}$ is a normalization constant, p is a radial index, $L_p^{|\,i\,|}(\cdot)$ is associated with the Laguerre polynomial, $w(z)$ is the beam width at distance z and is given by

$$w(z)=w_o\sqrt{1+(z/z_R)^2}, \tag{20}$$

where w_0 is the original beam width and z_R is Rayleigh range, defined as: $z_R=\pi w_o^2/\lambda$. $G_p^{|\,i\,|}(z)$ is the Gouy phase given as

$$G_p^{|l|}(z)=-i(2p+|l|+1)\tan^{-1}(z/z_R). \tag{21}$$

It should be noted that the scattered axial parameter z' varies only through the scattering angle θ. z is fixed in the following calculation.

Equations (11) and (19) are used to evaluate the scattering matrix of an x-ray of 1 nm wavelength and 1 μm waist width through a wide scattering angle range, $-\pi/2 < \theta < \pi/2$. It is assumed that there is no change in the Gouy phase through scattering.

Figure 4 illustrates the Compton scattering matrix value S versus scattering angle for several changes in OAM (Δl). The curves are generated by computing the normalized scattering matrix over the wide angle

range for four successive state changes in OAM. The normalized result in Fig. 2 can be interpreted as representing the probability of changing OAM state under Compton scattering. The results are bounded by the corresponding solid angle at which OAM states are invariant through Compton scattering. However, a change by just one-order state could happen with low probability, as the curve for $\Delta l = 1$ shows.

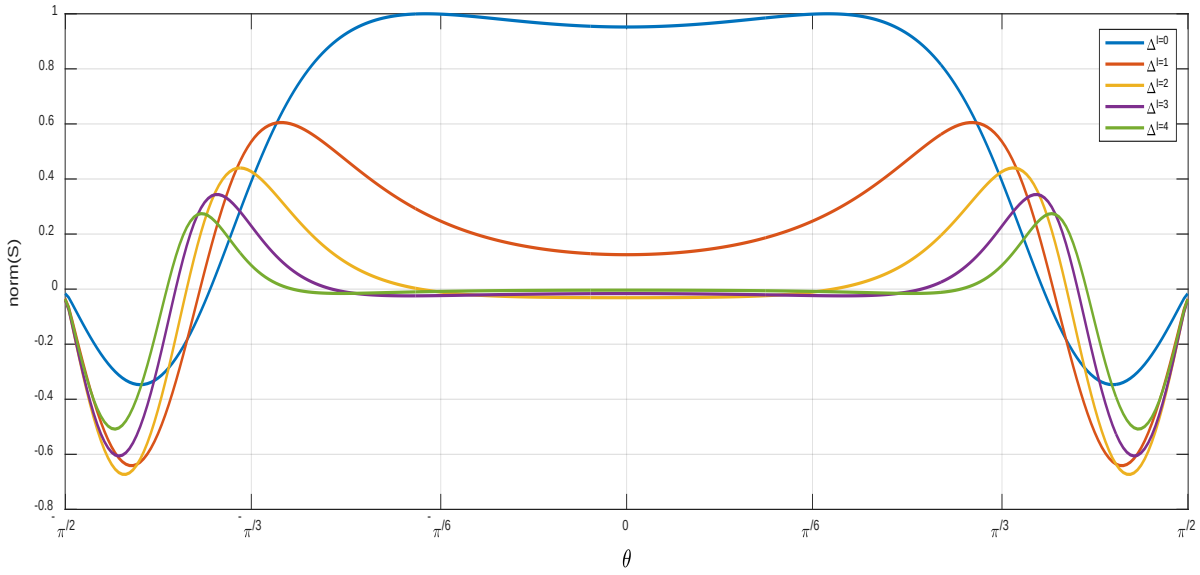

Figure 4. Normalized Compton scattering matrix versus scattering angle for an LG beam and small changes in OAM.

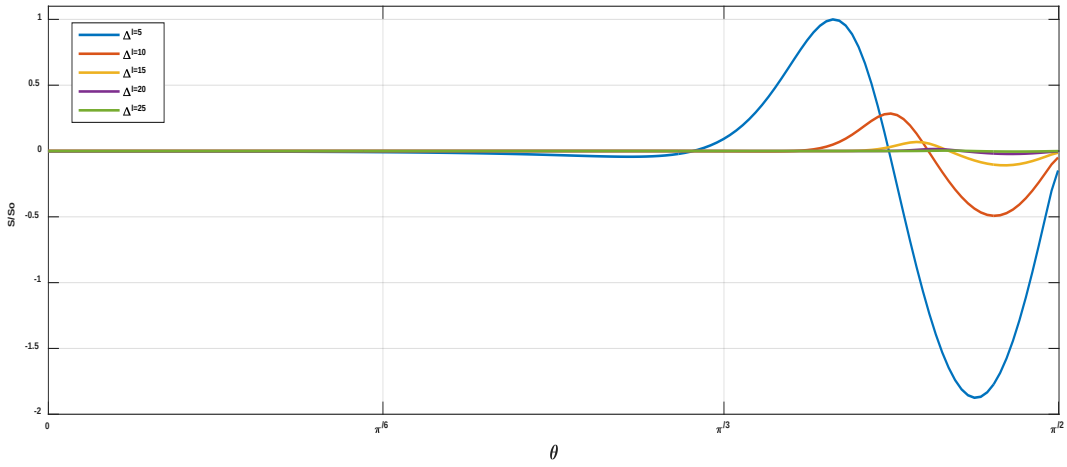

Figure 5. Normalized Compton scattering matrix versus scattering angle for an LG beam and large changes in OAM.

High probability of changing OAM states through scattering are represented by the peaks in Fig. 4. Scattering matrix elements are relatively small for higher change in OAM. This could be interpreted as a low probability for a large change in OAM due to Compton Scattering. Negative-value elements in Fig. 4 indicate the flipping of OAM states, and the curves indicate that scattering at wide angles can cause a flip

of the azimuthal phase. Consequently, OAM states are twisted "oppositely" for wide angle Compton-scattering. However; Scattering matrices are terminated at right angle scattering due to the minimization of the differential cross section of the Compton scattering process [28].

The scattering matrix norm is also calculated for large changes in photonic OAM states and the results are plotted in Fig. 5. This result again demonstrates the low probability of scattered twisted photons with large changes in their OAM. In addition, it indicates Compton scattering at wide angles is more likely to occur with the opposite twisted orientation. Dominant negative peaks in Fig. 5 represent a tendency for large changes in photonic OAM to be in an opposite orientation.

The other twisted light beam that is investigated is the Bessel Gaussian (BG) beam, which has a spatial wave given by [29]

$$R_l^{GB}(\rho,z) = A\exp\left[i\left(k-\frac{\kappa^2}{2k}\right)z - i\tan^{-1}\left(\frac{z}{z_R}\right)\right]J_l\left[\frac{\kappa\rho}{(1+iz/z_R)}\right]\exp\left[\left(\frac{-1}{w(z)^2}+\frac{ik}{2R(z)}\right)\left(\rho+\frac{\kappa^2}{k^2}z^2\right)\right], \quad (22)$$

where A is a normalization constant and R(z) is the phase front radius of curvature with

$$R(z) = z\sqrt{1+(z_R/z)^2}, \quad (23)$$

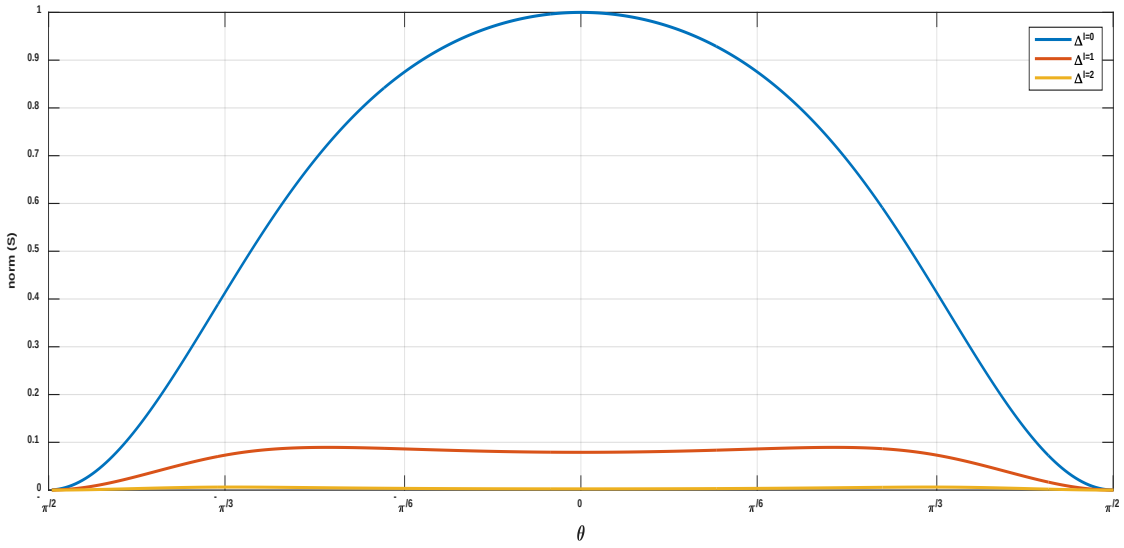

Figure 6. Normalized Compton scattering matrix norm versus scattering angle for the BG beam for several cases where OAM change is relatively small.

Equation (23) has been implanted in Eq. (11) to compute the corresponding scattering matrix with the same parameters – an x-ray source with 1 nm wavelength, 1 μm beam waist and constant Gouy phase. The associated scattering matrix is evaluated for first order changes in orbital angular as shown in Fig. 6. One can see that scattering matrix norm of the Bessel Gauss beam changes very slowly, with relatively higher values around scattering angle of $\pi/3$ compared with smaller values at small scattering angles, $|\theta| \leq \pi/6$, which is a similar result as the LG beam. The OAM of the BG beam tends to be invariant at small angle scattering and more variable in wide scattering. However the extreme minimum scattering element is at right angle scattering where the classical cross section is at minimum.

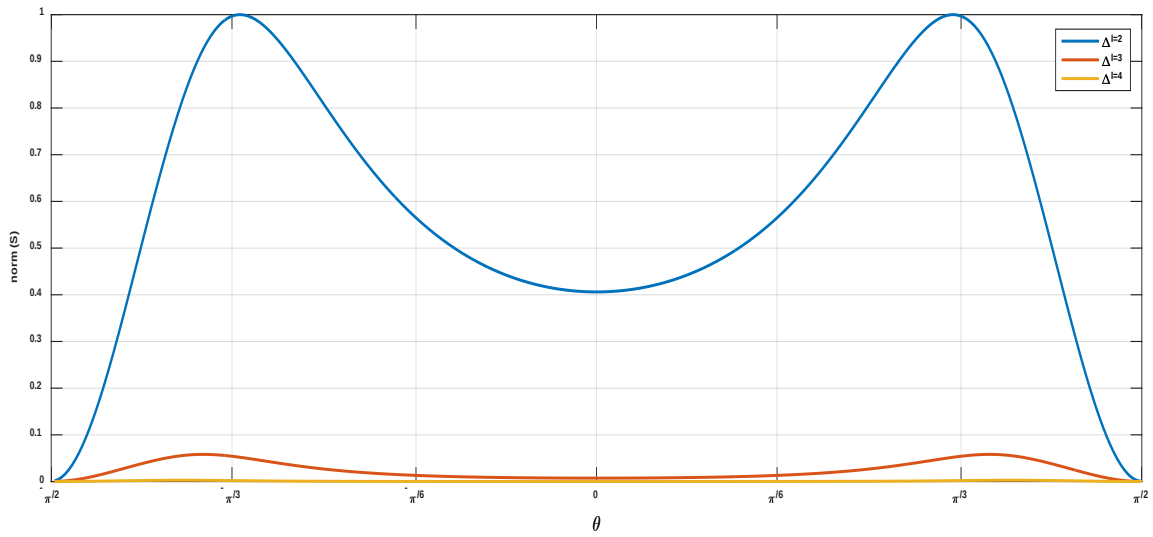

Figure 7. Normalized Compton scattering matrix norm versus scattering angle for the BG beam for several cases where OAM change is relatively large.

The scattering matrix is also examined for higher order changes in OAM of the Bessel Gaussian beam as illustrated in Fig. 7. The order is changed by varying associated the azimuthal parameter to 2, 3 and 4, respectively. The curves emphasize the high possibility of changing the OAM state under wide scattering conditions compared with small angle scattering.

4.2 Design of a plasmonic metasurface to measure OAM.

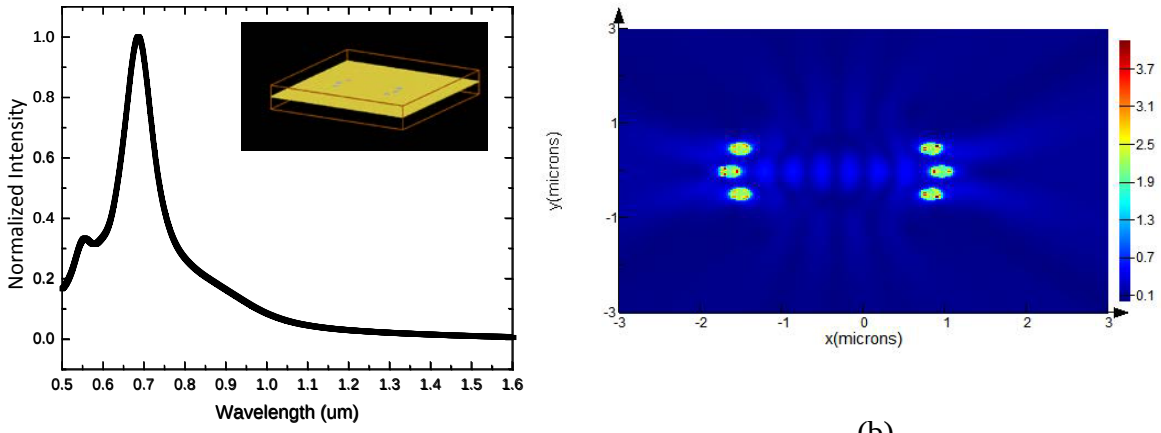

(a) (b)

Figure 8. Example calculated spectral response at wavelength 678 nm (a) normalized transmittance versus wavelength. The inset shows a schematic of the metasurface. (b) the electric field distribution on the metasurface.

With the proposed metasurface structure, the optical vortex beam can be detected by monitoring the near-field pattern of the metasurface. Fig. 8 shows an example of the calculated spectral response for a particular metasurface design at $\lambda = 678$ nm. For the purpose of demonstration, the display in Fig. 8 (b) shows the field distribution on the device when there is resonance and a standing wave at its center. In

Fig. 8(a), we observe that there is sharp peak intensity approximately at the wavelength. The presence of the feature is interpreted as arising from Fabry-Perot resonance that is created by the reflectance and transmittance properties of the metasurface structure. The inset presents the three-dimensional metasurface profile which is at the several micrometer order. The corresponding electric field distribution is illustrated in Fig. 8(b), showing the selective excitation of the surface plasmon waves. The structure and corresponding calculated response spectra of the metasurface is implemented using a finite-element-method solver and COMSOL Multiphysics software.

5.0 CONCLUSIONS

The conversation of OAM at Compton scattering was analyzed. The norm of the scattering matrix for twisted light that is scattered by atomic electrons was calculated. The results indicate that the OAM of a twisted light can be changed through Compton scattering. Specific numerical values were determined for Compton scattering of Laguerre Gaussian and Bessel Gaussian light beams. It was concluded from the analysis that OAM states were invariant at forward scattering at small angle scattering but could vary significantly at wide angle scattering.

A compact and efficient approach was proposed to detect vortex beams with OAM using plasmonic metasurfaces. An example metasurface structure that couples normally incident optical vortex beams into to resonant plasmon waves was depicted. The example calculated spectra response was presented and further electromagnetic simulations can be performed using the finite-difference time-domain solver and COMSOL software. This study provided an important step towards the development a highly compact OAM detector.

6.0 REFERENCES

[1]. L. Allen, M. W. Beijersbergen, R. J. C. Spreeuw, J. P. Woerdman, “Orbital angular momentum of light and the transformation of Laguerre-Gaussian laser modes,” Phys. Rev. A, 45(11), 8185-8189 (1992).

[2]. S. M. Zhao, J. Leach, L. Y. Gong, J. Ding, B. Y. Zheng, “Aberration correction for free-space optical communications in atmosphere turbulence using orbital angular momentum states,” Opt. Exp., 20(1), 452-461 (2012).

[3]. J. A. Anguita, “Orbital angular momentum distribution in a multi-vortex free-space optical link,” Frontiers in Optics, 2009.

[4]. C. Paterson, “Atmospheric turbulence and orbital angular momentum of single photons for optical communications,” Phys. Rev. Lett., 94(15), 153901 (2005).

[5]. X. Sheng, Y. Zhang, X. Wang, Z. Wang, Y. Zhu, “The effects of non-Kolmogorov turbulence on the orbital angular momentum of a photon-beam propagation in a slant channel,” Opt. Quant. Electron. 43, 121-127 (2012).

[6]. Y. Zhang, Y. Wang, J. Xu, J. Wang, J. Jia, “Orbital angular momentum crosstalk of single photons propagation in a slant non-Kolmogorov turbulence channel,” Opt. Comm., 284, 1132-1138 (2011).

[7]. R. W. Boyd, B. Rodenburg, M. Mirhosseini, S. M. Barnett, “Influence of atmospheric turbulence on the propagation of quantum states of light using plane-wave encoding,” Opt. Exp., 19(19), 18310-18316 (2011).

[8]. A. Mair, A. Vaziri, G. Weihs, A. Zeilinger, “Entanglement of the orbital angular momentum states of photons,” Nature, 412, 313-316 (2001).

[9]. D. J. Sanchez and D. W. Oesch, “Orbital angular momentum in optical waves propagating through distributed atmospheric turbulence,” Opt. Express 19, 24596–24068 (2011).
[10]. D. W. Oesch, D. J. Sanchez, “Creating well-defined orbital angular momentum states with a random turbulent medium,” Opt. Express 20, 12292-12302 (2012).
[11]. D. W. Oesch, D. J. Sanchez, C. M. Tewksbury-Christle, and P. R. Kelly, “The aggregate behavior of branch points- altitude and strength of atmospheric turbulence layers,” Proc. SPIE 7816, 0501–0513 (2010).
[12]. Y. Miyamoto, D. Kawase, M. Takeda, K. Sasaki, S. Takeuchi, “Detection of superposition in the orbital angular momentum of photons without excess components and its application in the verification of non-classical correlation,” J. Opt., 13, 064027 (2011).
[13]. J. H. Park, C. H. Kim, J. W. Rhim, J. H. Han, “Detecting chiral orbital angular momentum by circular dichrosim ARPES,” arXiv:1112.1821 (December 2011)
[14]. H. Wei, X. Xue, J. Leach, M. J. Padgett, S. M. Barnett, S. Franke-Arnold, E. Yao, J. Courtial, “Simplified measurement of the orbital angular momentum of single photons,” Opt. Comm., 223, 117-122 (2003).
[15]. J. Leach, M. J. Padgett. S. M. Barnett, S. Franke-Arnold, J. Coutial, “Measuring the orbital angular momentum of a single photon,” Phys. Rev. Lett., 88(25), 257901 (2002).
[16]. B. S. Davis, L. Kaplan, and J. H. McGuire, “On Exchange of Orbital Angular Momentum Between Twisted Photons and Atomic Electrons”, J. Opt. **15** 109501 (2013).
[17]. M. Padgett and L. Allen, “Light with a twist in its tail”, Cont. Phys. **41**(5), 275-285 (2010).
[18]. A. H. Compton, “A Quantum Theory of the Scattering of X-Rays by Light Elements”, Phys Rev. **21**(5), 483–502 (1923).
[19]. A. Liu, X. Xiong, X. Ren, Y. Cai, G. Rui, Q. Zhan, G. Guo, G. Guo, “Detecting orbital angular momentum through division-of-amplitude interference with a circular plasmonic lens”, Scientific Reports, **3**, 2402 (2013).
[20]. P. Genevet, J. Lin, M. A. Kats, F. Capasso, “Holographic detection of the orbital angular momentum of light with plasmonic photodiodes”, Nature Communications, 3, 1278 (2012).
[21]. D. A. Smirnova, A. E. Miroshnichenko, Y. S. kivshar, A. B. Khanikaev, “Tunable nonlinear graphene metasurfaces”, Phys. Rev. B 92, 161406 (R) (2015).
[22]. Z. Li, K. yao, F. Xia, S. Shen, J. Tian, Y. Liu, “Graphene plasmonic metasurfaces to steer infrared light,” Scientific Reports, 5, 12423 (2015).
[23]. N. Yu, P. Genevet, F. Aieta, M. A. Kats, et. al, “Flat optics: Controlling wavefronts with optical antenna metasurfaces”, IEEE Journal of Selected Topics in Quantum Electronics, 19(3), 4700423 (2013).
[24]. M. S. Dresselhaus, Solid State Physics, Part II: Optical Properties of Solids. Chapter 3, 15-23 (2001).
[25]. M. Nairat and D. Voelz, “Compton scattering of a twisted light,” Submitted to J. Opt, JOPT-103724, 10/23/2016.
[26]. X. Xiao, S. Y. Cho, D. G. Voelz, C. Pelzman, “Detection of optical vortex beams using plasmonic metasurfaces”, in Imaging and Applied Optics, OSA Technical Digest (online) (Optical Society of America, 2016), paper W2A.5.
[27]. L. Allen, V. E. Lembessis, M. Babiker “Spin-orbit coupling in free-space Laguerre-Gaussian light beams”, Phys. Rev. A 53(5), R2937-R2939 (1996).
[28]. Klein, O; Nishina, Y. "Über die Streuung von Strahlung durch freie Elektronen nach der neuen relativistischen Quantendynamik von Dirac". *Z. Phys.* **52** (11), 853-868 (1929).

[29]. I. A. Litvin, M. G. McLaren and A. Forbes “Compton scattering of twisted light: angular distribution and polarization of scattered photons”, Proc. SPIE 7062, Laser Beam Shaping IX, 706218 (2008).

APPENDIX- Presentations and Publications Resulting from this Research.

A. M. Nairat and D. Voelz, “Compton scattering of a twisted light,” Submitted to J. Opt, JOPT-103724, 10/23/2016.
B. X. Xiao, S. Y. Cho, D. G. Voelz, C. Pelzman, “Detection of optical vortex beams using plasmonic metasurfaces”, in Imaging and Applied Optics, OSA Technical Digest (online) (Optical Society of America, 2016), paper W2A.5.

LIST OF ABBREVIATIONS

BG	Bessel Gaussian
LG	Laguerre Gaussian
OAM	Orbital Angular Momentum
SPP	Surface Plasmon Polariton

DISTRIBUTION LIST

DTIC/OCP
8725 John J. Kingman Rd, Suite 0944
Ft Belvoir, VA 22060-6218 1 cy

AFRL/RVIL
Kirtland AFB, NM 87117-5776 1 cy

WUM

Official Record Copy
AFRL/RDSS 1 cy